NASA Technical Memorandum 7(

(NASA-TM-78595) FUEL-CONSERVATIVE GUIDANCE SYSTEM FOR POWERED-LIFT AIRCRAFT (NASA) 18 p HC A02/MF A01 CSCL 01C

N79-26009

Unclas
G3/01 23484

Fuel-Conservative Guidance System for Powered-Lift Aircraft

Heinz Erzberger and John D. McLean

June 1979

National Aeronautics and
Space Administration

NASA Technical Memorandum 78595

Fuel-Conservative Guidance System for Powered-Lift Aircraft

Heinz Erzberger
John D. McLean, Ames Research Center, Moffett Field, California

NASA
National Aeronautics and
Space Administration

Ames Research Center
Moffett Field, California 94035

FUEL-CONSERVATIVE GUIDANCE SYSTEM FOR POWERED-LIFT AIRCRAFT

Heinz Erzberger* and John D. McLean*
Ames Research Center, NASA, Moffett Field, California

Abstract

A concept for automatic terminal-area guidance, comprising two modes of operation, has been developed and evaluated in flight tests. In the first or predictive mode, fuel-efficient approach trajectories are synthesized in fast time. In the second or tracking mode, the synthesized trajectories are reconstructed and tracked automatically. An energy rate performance model derived from the lift, drag, and propulsion-system characteristics of the aircraft is used in the synthesis algorithm. The method optimizes the trajectory for the initial aircraft position and wind and temperature profiles encountered during each landing approach. The paper describes the design theory and discusses the results of simulations and flight tests using the Augmentor Wing Jet STOL Research Aircraft.

List of Symbols

D	= drag force, lb
d_b, d_f	= distance of backward and forward integration, respectively
d_c	= cruise distance, ft
d_h	= length of ground track from initial to final position of aircraft, ft
E	= energy, ft
$\dot{E}_n$	= energy rate, ft/sec
$\dot{E}_{nmax}$, $\dot{E}_{nmin}$	= maximum and minimum available energy rate, respectively, ft/sec
F, G	= perturbation state and control distribution matrices, respectively
g	= acceleration of gravity, ft/sec^2
h	= altitude, ft
h_f, h_i	= final and initial altitudes of aircraft, respectively, ft
K	= feedback gain matrix
$k_{\phi y}$, $k_{\phi \dot{y}}$	= lateral error and error rate feedback gains
L	= lift force, lb
$\dot{S}$	= speed along ground track, ft/sec
T	= thrust force, lb
t	= time, sec
u	= perturbation control vector
u_c	= aircraft control vector
V_a	= airspeed, ft/sec or knots
V_{af}, V_{ai}	= final and initial airspeeds of aircraft, respectively, ft/sec or knots
V_w	= wind speed in direction of ground track, knots
W	= aircraft weight, lb
x	= perturbation state vector
x_f, x_i	= final and initial x coordinates of aircraft, respectively, ft
y_f, y_i	= final and initial y coordinates of aircraft, respectively, ft
α	= angle of attack, deg
γ	= inertial flight-path angle, deg
γ_a	= Aerodynamic flight-path angle, rad or deg
$\Delta\dot{V}_a$	= airspeed rate correction due to wind shear, ft/sec^2
Δ_y	= crosstrack error, ft
$\Delta_{\dot{y}}$	= crosstrack error rate, ft/sec
δ_f	= flap angle, deg
δ_{fmax}	= maximum flap angle, deg
ε	= fraction of energy rate used for changing speed
θ_c	= command pitch angle, deg
ν	= vectored thrust, in degrees of nozzle angle
π	= throttle setting, in percent RPM
σ	= fraction of available energy rate
ϕ_c, ϕ_r	= commanded and reference bank angles, respectively, deg
ψ_f, ψ_i	= final and initial ground heading of aircraft, respectively, deg

Introduction

In the past, terminal-area guidance system design for aircraft has concentrated primarily on automatic glide slope tracking, flare, and touchdown. During recent years, designs have been developed to provide automatic guidance along curved and decelerating approach paths.[1] This increased capability was made possible through the integration of digital computers into the flight guidance system. However, even in the more advanced designs, automatic

*Research Scientist. Member AIAA.

guidance is limited to a few prestored three-dimensional flight paths, as in Ref. 1. While the ability to fly complex prestored trajectories is essential, it cannot give optimum performance under actual terminal-area operating conditions as shall be explained.

First, a prestored trajectory cannot optimize fuel consumption or a similar performance measure under actual operating conditions. Optimum trajectories depend significantly on aircraft gross weight, wind and temperature profiles, and on the initial state of the aircraft. These variables cannot be predicted with the required precision prior to takeoff. To prestore optimum trajectories for each of the conditions likely to be encountered would result in an impossibly large memory requirement. Therefore, prestored trajectories must necessarily represent a compromise in performance.

Second, in existing systems the pilot must fly the aircraft manually from its current position to the starting point of the trajectory. This flight segment is known as the capturing maneuver. Three-dimensional, curved trajectories can be difficult to capture manually, and, if the trajectory also includes a specification of landing time, as is the case in 4D guidance, the capturing maneuver cannot be done by the pilot without computer assistance. Therefore, the capturing maneuver, because of its variability, can only be generated by onboard trajectory synthesis.

Third, aircraft in high density airspace are usually controlled by air traffic control vectors and during this period cannot follow a prestored flight path. Synthesis of a trajectory can only begin after the aircraft has received its final vector and has been cleared for approach. But the initial position of the aircraft at that time varies between approaches, thus trajections require onboard synthesis.

An initial design of a four-dimensional guidance system embodying the concept of onboard trajectory synthesis, including an advanced capture law, was developed and flight tested onboard a Convair 340 aircraft equipped with the STOLAND avionics.[2] In the design described here, horizontal trajectories are generated by the method of Reference 2, but vertical and speed profiles are synthesized using simplified aero/propulsion performance models of the aircraft. This results in profiles that are optimum for fuel conservation. Design of the control law for tracking the synthesized trajectory is based on the linearized perturbation guidance approach. Since the perturbation equations are aircraft configuration-dependent, gain scheduling is used in the feedback law.

The Augmentor Wing Jet STOl Research Aircraft (AWJSRA) was chosen as the test vehicle for this concept. This type of powered-lift aircraft is highly cost-sensitive to operational procedures in the terminal area. It also exemplifies particularly well the unique problems of powered-lift aircraft, namely, high fuel consumption in the STOL mode; dependence of both lift and drag on thrust; and an excess of controls over the minimum number needed to determine path and speed. These factors suggest that trajectory optimization could greatly increase the operational efficiency of the aircraft. Implementation of this concept was facilitated by the existing installation of the STOLAND avionics system onboard the aircraft.

Energy Rate Model and Selection of Reference Controls

An energy rate model of aircraft performance has been found to yield a compact and sufficiently accurate representation of performance for terminal-area trajectory synthesis. In this section a performance model based on energy rate is derived and then applied to determine the optimum reference controls for synthesizing trajectories.

Consider the standard expression for energy rate written as

$$\frac{dE}{dt} = \frac{(T - D)V_a}{W} \tag{1}$$

where

$$E = h + \frac{1}{2g} V_a^2 \tag{2}$$

with constraint $L = W$ (Ref. 3). It is assumed throughout this paper that flight-path angles are small such that $\cos \gamma_a \approx 1$ and $\sin \gamma_a \approx \gamma_a$. Furthermore, it is assumed that flight-path angle rates are so small that their effect on lift is negligible. Differentiation of Eq. (2) with respect to time gives an equivalent expression for energy rate:

$$\frac{dE}{dt} = \frac{dh}{dt} + \frac{1}{g} V_a \frac{dV_a}{dt} \tag{3}$$

Equations (1) and (3) can be nondimensionalized by dividing them both by V_a. The resulting quantity on the left side, $(1/V_a)(dE/dt)$, is defined as the normalized energy rate $\dot{E}_n$, or energy rate for short. By using the relation $(dh/dt) \approx V_a\gamma_a$, the two relations for $\dot{E}_n$ become

$$\dot{E}_n = \frac{T - D}{W} \tag{4}$$

$$\dot{E}_n = \gamma_a + \frac{1}{g}\frac{dV_a}{dt} \tag{5}$$

with constraint $L = W$.

Equation (4) specifies the energy rate as a function of the difference between thrust and drag, subject to the constraint that lift equal weight. Thrust and drag are in turn functions of the controls producing forces in the flight-path direction, namely throttle π, flap angle δ_f, nozzle angle ν (vectored thrust), and angle of attack α. Equation (5) determines the relationship between flight-path angle and acceleration for the energy rate calculated from Eq. (4). Equation (5) indicates that, in particular, a given energy rate may be utilized to fly at flight-path angle γ_a with constant airspeed, or to fly at zero flight-path angle with acceleration dV_a/dt. An infinity of other combinations of γ_a and dV_a/dt can also be chosen to yield the same energy rate. This makes possible a simplifying dichotomy in the trajectory synthesis, namely, at any time the desired energy rate is selected first by choice of appropriate controls and then the linearly related quantities of γ_a and dV_a/dt are selected to generate the specifics of the flight path. The next section develops the complete synthesis algorithm based on this approach. Here we elaborate on the determination of the functional dependence of energy rate on the force-producing controls.

Since the STOL aircraft studied in this paper has four controls to achieve a specified energy rate and to maintain lift equal to weight, there is an excess of two controls over the minimum number needed for a simultaneous solution to Eq. (4) and the constraint $L = W$. These two extra degrees of freedom in the controls are exploited to minimize power setting and, therefore, fuel flow at every energy rate. This optimization problem is restated in equivalent form as the maximization of energy rate for a given power setting:

$$\dot{E}_n(\pi) = \max_{\nu,\alpha,\delta_f} \frac{T - D}{W} \qquad (6)$$

$$\text{Constraint:} \quad L(\pi,\nu,\alpha,\delta_f) = W \qquad (7)$$

The maximization must obey various inequality constraints on the controls:

$$-10.5° < \alpha < 19.5°$$

$$6° < \nu < 100°$$

$$5.6° < \delta_f < \delta_{fmax}(V_a) \qquad \text{[Flap placard]}$$

In addition, a lift or maneuver margin must be satisfied at every point to guarantee sufficient normal force for changing the flight path. Pilots familiar with this aircraft specify that at least 0.4 g of normal acceleration must be attainable at any time by an increase in the angle of attack alone.

The use of Eq. (6) results in the selection of the controls that yield the maximum attainable energy rate at each thrust setting. This ensures the efficient use of thrust at any energy rate that requires more than the minimum thrust. But energy rates more negative than those attainable by Eq. (6) are also of interest. Such negative energy rates must occur at the greater of minimum or idle thrusts required by the maneuver margin. At a particular airspeed, a decrease in the energy rate below the minimum attained through Eq. (6) can be effected by increasing the vectored thrust angle ν and/or the flap angle δ_f. The third control, angle of attack α, is needed to satisfy the constraint $L = W$. The two degrees of freedom in the controls can be exploited to minimize noise exposure along the ground track. Noise under the aircraft is known to increase as the nozzles producing the vectored thrust are turned downward. Therefore, a further decrease in energy rate is achieved by first increasing flap angle until it reaches its limit or placard value and only then by increasing nozzle angle.

The result of applying these procedures to the AWJSRA is shown in Fig. 1 for a weight of 38,000 lb, sea-level altitude, and standard temperature. The figure gives the envelope of energy rate vs indicated airspeed with throttle, flaps, and vectoring nozzle as parameters. Angle of attack is not plotted to avoid cluttering the figure. At any airspeed, the $\dot{E}_{nmax}$ and $\dot{E}_{nmin}$ curves define the range of permissible energy rates. The optimum controls for a given airspeed and energy rate are determined by interpolation between contours of constant controls. For example, at an airspeed of 105 knots and $\dot{E}_n = -0.17$, the optimum controls are found to be: $\delta_f = 26°$, $\nu = 6°$, $\pi = 84\%$ (point A, Fig. 1). Angle of attack (not shown) is 8.4°. Maximum energy rate with minimum thrust occurs at 112 knots (point B) and corresponds approximately to $(L/D)_{max} \approx 10$.

It should be noted that the force-producing controls in this experimental STOL aircraft have unusual characteristics that account for the relative complexity of Fig. 1. Throttle affects both lift and drag at all speeds, but the effect on lift is greatest in the STOL regime below about 80 knots. The thrust magnitude produced by the vectoring nozzle, referred to as the hot thrust, is also controlled by the throttle and accounts for about 60% of the total thrust produced by the two engines. The remaining 40% of the thrust which is the cold thrust produced by the fans, energizes the augmentor wing to increase lift at STOL speeds.

The relationship between the controls and the energy rate is revealed more clearly in Fig. (2) at the example airspeed of 105 knots. Many such plots at various airspeeds would be required to illustrate the complete dependence of the controls on energy rate. As the energy rate decreases below its maximum value of 0.28, throttle decreases nearly linearly until idle throttle is reached. In this interval flaps increase only slightly while nozzle angle remains at minimum and angle of attack increases. At more negative energy rates, flaps become the dominant control until they reach the placard value of 40° at this airspeed. Angle of attack decreases sharply as flap angle increases. Finally, nozzle angle increases toward its maximum value of 100° as the energy rate decreases toward its negative limit of -0.3.

In the flight implementation of the algorithm, four diagrams as shown in Fig. 1 are utilized, two for sea-level altitude at weights of 38,000 and 48,000 lb and two others for 5000-ft altitude at similar weights. Experience indicates that these are sufficient data to interpolate the controls adequately. Each diagram requires 124 words of memory in the airborne computer. The small circles in Fig. 1 indicate the locations of points that are stored. The energy rate data are also corrected for deviations from the standard temperature profile. Correction is done by computing a thrust setting corrected for temperature deviations.

Synthesis of Complete Profiles

In the preceding section the criteria of fuel conservation and noise reduction were used to determine the four reference controls of throttle, nozzle angle, flap angle, and angle of attack as functions of the energy rate. This approach replaced the problem of selecting four control variables with the simpler problem of selecting a single, equivalent variable, namely, the energy rate. In this section we make use of the energy rate variable in generating efficient terminal-area trajectories.

The problem of terminal-area-trajectory synthesis can be stated as the specification of rules for flying an aircraft with initial state vector $[x_i, y_i, h_i, \psi_i, V_{ai}]$ to a final state vector $[x_f, y_f, h_f, \psi_f, V_{af}]$. To be of practical interest, such rules must generate efficient and flyable trajectories connecting various initial and final state vectors. By specifying a performance criterion such as fuel consumption, we can fit this problem into the framework of optimal control theory. However, the difficulty of solving an optimal control problem characterized by a five-element state vector makes this approach computationally impractical for in-flight implementation. Following Ref. 4, we have adopted the simplifying procedure of separating the synthesis problem into two essentially independent problems.

The first problem consists of synthesizing the horizontal or 2D trajectory. References 4 and 5 give several algorithms for computing near-minimum-distance 2D trajectories as a sequence of an initial constant radius turn, straight flight, and a final constant radius turn, where the turn radii are chosen so as to avoid exceeding a specified maximum bank angle at the maximum ground speed encountered in each turn. A description of the algorithm used in the flight implementation can be found in Ref. (5). Figure 3 illustrates the 2D trajectories computed by the algorithm for several initial positions, P_i, in the terminal area. Note that the terminal point, P_f, lies on an extension of the runway centerline, and that the heading angle ψ_f of all trajectories is equal to the runway heading at that point. Thus, the algorithm always generates 2D trajectories that match the initial and final state vector components x_i, y_i, ψ_i and x_f, y_f, ψ_f.

The second problem, solved after the horizontal trajectory has been computed, consists of synthesizing efficient speed and altitude profiles which match the initial and final speeds and altitudes V_i, h_i, and V_f, h_f, respectively.

The horizontal distance of the trajectory d_h, a known quantity computed in the previous step, adds a third boundary condition to be satisfied by the profiles. While this three-state optimal-control problem is much simpler to solve than the original five-state problem, it is still too complex for onboard-computer implementation. A simpler algorithm was therefore developed that generates near-optimum speed-altitude profiles by matching the general characteristics of optimum fuel and noise trajectories studied in Refs. 6 and 7, respectively. We briefly explain the rationale for this algorithm with reference to descent, which is the most difficult case.

It was found in Ref. 6 that the descent portion of a minimum fuel descent trajectory is characterized by a delay in the start of the energy decrease as long as possible consistent with meeting end constraints of speed and altitude. Furthermore, the energy change consists initially of descent to the final altitude at near-constant indicated airspeed followed by a rapid airspeed deceleration in level flight. **Most of the energy change takes place at minimum throttle, as one might expect for minimum fuel flight. Minimum noise descent profiles computed in Ref. 7 are similar in that they also delay the start of energy decrease as long as possible, but they approach the final altitude in a steep descent to maximize the aircraft's altitude above the ground near the runway. This means that the deceleration to the final airspeed takes place before the start of descent or during the early portion of the descent. Thus the two types of descent profiles differ primarily in the way they proportion the use of available energy rate to decrease altitude and airspeed.**

To facilitate the synthesis of such profiles, a family of decreasing (and by extension, increasing) energy profiles, which include the two types described as special cases, is defined by two parameters, σ and ε. The first parameter, σ, selects the fraction of minimum/maximum available energy rate, $\dot{E}_{nmin}$, ($\dot{E}_{nmax}$) to be used for decreasing/increasing energy. The values of $\dot{E}_{nmin}$ and $\dot{E}_{nmax}$ can be read from Fig. 1 at each indicated airspeed. The second parameter, ε, determines the fraction of the selected energy rate to be used for deceleration/acceleration. Then, for particular choices of σ and ε, the energy rate, airspeed, flight-path angle, altitude, and horizontal distance are computed as follows:

$$\dot{E}_n = \sigma \dot{E}_{nmin} \qquad 0 \leq \sigma \leq 1 \tag{7}$$

$$\dot{V}_a = g \varepsilon \dot{E}_n \qquad 0 \leq \varepsilon \leq 1 \tag{8}$$

$$\gamma_a = (1 - \varepsilon) \dot{E}_n \tag{9}$$

$$\dot{h} = V_a \gamma_a \tag{10}$$

$$\dot{S} = V_a \cos \gamma_a + V_w \tag{11}$$

where V_w is the along-track component of wind speed. Note that Eqs. (7)-(9) are consistent with Eqs. (4) and (5) for all values of σ and ε. Decreasing/increasing energy profiles are generated by integrating Eqs. (8), (10), and (11) for particular choices of σ and ε.

To illustrate the effect of the parameter ε on the descent/deceleration profiles, assume $\dot{E}_n = -0.13$, independent of speed, and let the airspeed to be achieved at touchdown be 100 ft/sec. To achieve the desired boundary conditions, Eqs. (8), (10), and (11) are integrated in backward time starting with the speed and altitude at touchdown. The resulting airspeed and altitude profiles are plotted as a function of distance to touchdown in Fig. 4 for $\varepsilon = 1$, 0.5, 0.0. The profile for $\varepsilon = 1$ is seen to approximate the minimum fuel, for $\varepsilon = 0$, the minimum noise descent, and for $\varepsilon = 0.5$, a compromise between fuel and noise minimization.

To achieve minimum fuel or noise performance, changes in energy should be made at maximum rate. This is accomplished by setting σ to unity and thereby following the $\dot{E}_{nmin}$ contour during descent and deceleration. However, for the aircraft under study this yields energy rates too negative for safe operation in the terminal area at some airspeeds. A limit less than one is also necessary to reserve energy rate for perturbation control. A practical upper limit on σ is about 0.9 for the AWJSRA. In the flight implementation, the two profile parameters are keyboard entries that allow the pilot to choose values appropriate for each landing approach. In addition, the pilot can specify the maximum deceleration and descent angles via keyboard entry. The maximum safe deceleration for this aircraft is limited to about 0.06 g by the maximum rate at which flaps can be extended. The synthesis algorithm is configured to decrease σ below its limit if that is necessary to satisfy these constraints.

The backward time integration described above generates an increasing (in backward time) energy-profile starting at the desired final speed and altitude. To complete the synthesis of the descent trajectory we still need rules for matching this profile to the initial speed and altitude of the aircraft. The freedom of the aircraft to maneuver in altitude is restricted by air traffic control as well as passenger comfort considerations. Thus, as an aircraft approaches a terminal area, it is generally not allowed to climb above its initial approach altitude for the purpose of optimizing the approach trajectory. The aircraft must hold this altitude until starting the final descent. However,

while flying at altitude h_i, it may change to a new airspeed, V_{at} called the terminal-area speed which can be higher or lower than the initial speed V_{ai}. Unless specified by the pilot via keyboard entry, it is chosen to minimize fuel use per unit distance, and is 140 knots for this aircraft (it would be 220-250 knots for conventional jet transports).

The various rules contained in the preceding two paragraphs can now be combined to yield the complete algorithm. The synthesis begins with the backward time integration from final conditions h_f, V_{af} using the specified σ and ε. If the altitude reaches its target value of h_i before the airspeed reaches its target value of V_{at}, we set $\varepsilon = 1$ and then continue the backward time integration until the airspeed has also achieved its target value. When setting $\varepsilon = 1$, the flight-path angle is forced to zero and the energy rate is used entirely for accelerating (in backward time) toward V_{at}. On the other hand, if the airspeed reaches its target value before the altitude does, we set $\varepsilon = 0$. This stops the airspeed change and uses the energy rate entirely for increasing the altitude toward its target value of h_i. When the second and last variable reaches its target value, we set $\sigma = 0$, i.e., $\dot{E}_n = 0$, thus completing the backward time integration. Next, we begin a forward time integration to get the distance required to change speed from V_{ai} to V_{at} with $\varepsilon = 1$. Let the distances for the backward and forward integrations be d_b and d_f, respectively. A valid trajectory has been generated if the cruise distance d_c, computed from

$$d_c = d_h - d_b - d_f \tag{12}$$

is nonnegative, i.e., $d_c \geq 0$. If d_c is negative, the synthesis has failed because the aircraft is too close to the capture point P_f.

Figure 5 illustrates the various segments of an approach trajectory synthesized by the algorithm. As before, we assume for simplicity that $\dot{E}_n = -0.13$, a constant. Other parameters defining the problem are indicated in the figure. Note that the initial descent at $\gamma_a = -7.5$ shallows to $\gamma_a = -3.75$ to allow the aircraft to decelerate. The reference controls for this trajectory can be interpolated from Fig. 1.

We conclude this section by mentioning briefly other important features of the algorithm included in the flight implementation. The airspeed deceleration is corrected for known wind shears, which are computed from a knowledge of $V_w(h)$ if available. The wind shear correction factor is

$$\Delta\dot{V}_a = -(dV_w/dh)V_a\gamma_a \tag{13}$$

and is added to the right side of Eq. (8) to obtain the corrected airspeed rate. Furthermore, the reference controls are corrected for the effect of the bank angle used in flying a turn by interpolating the controls at an aircraft weight multiplied by the load factor $1/\cos\phi$. Integration step size varies during synthesis. During decelerations or accelerations it is 1 sec while during altitude changes at fixed speed it is 5 sec. Total time for synthesizing a complete trajectory consisting of a horizontal trajectory similar to the ones shown in Fig. 3 and a speed/altitude profile similar to the one in Fig. 5 is about 2 sec on the Sperry Flight Systems 1819A airborne computer used in the flight tests. When the trajectory synthesis is time-shared with navigation and other necessary computations, the computing time increases to about 6 sec.

Real-Time Profile Generation

After a profile has been synthesized in fast time and the pilot has elected to fly it, the reference states and controls for that profile must be generated in real time. The synthesized profile can contain discontinuous changes in roll and pitch angle and throttle and vectoring nozzle position at "command points" where changes in speed, altitude, or heading are initiated or terminated. The real time profile generation therefore must provide a certain amount of lead time to these control variables to minimize tracking errors at command points. These functions are performed by the Real-Time Profile Generation Logic.

If an on-board computer has sufficient memory capacity to store all of the reference states and controls during fast time synthesis at small intervals of time, this logic would be relatively simple. However, limitations on the storage available in the STOLAND computer mode this approach impractical. To minimize memory usage, a different method was implemented at the expense of increased complexity of computation. The method consists of storing reference trajectory data, i.e., control positions, speed, altitude, etc., only at the "command points," as defined earlier. Between "command points" the reference trajectory is generated in real time by the same integration logic used during fast time synthesis; however, the integration is now done entirely in forward time. Generation of a flyable reference trajectory that meets the desired boundary conditions is guaranteed because it is a precise repetition of a previously successful synthesis.

The real-time forward integration uses distance along the ground track as the independent variable. The integrated or dependent variables are reference time, airspeed, altitude, and heading. The choice of distance rather than time gives a more flexible and operationally improved system for the following reasons. In a distance-based reference trajectory system, the aircraft will track the reference airspeed and altitude regardless of winds as it flies along the ground track. It is not necessary to null time errors if time control is not required. The system can thus be operated either in a 3D- or a 4D-tracking mode, depending on whether the time error loop is open or closed. This flexibility is lacking in a time-based reference trajectory system, where only the 4D tracking mode is possible. In the time-based system, if the actual winds differ significantly from the forecast winds used in fast-time trajectory synthesis, the aircraft controls may have insufficient authority to track the reference position resulting in unacceptable tracking characteristics.

One difficulty with the distance-based reference trajectory is that distance along the trajectory does not necessarily increase monotonically with time. Large navigation errors can cause the new reference position to fall behind the previous one or to move ahead with a large step. This can result in control system saturation during the critical descent and deceleration segments. The system therefore contains logic that prevents the reference position from backing up or from advancing faster than about 1.5 times the current ground speed between position updates, which occur at 100 msec intervals.

Perturbation Guidance Law

Perturbations of the aircraft states from the reference states are used in the guidance law to generate perturbation controls which are added to the reference controls in order to null errors in airspeed, altitude, and crosstrack position. The feedback states in the guidance law also include crosstrack error rate and flight-path angle as well as the integrals of airspeed and altitude errors. The latter two are used to reduce speed and altitude bias errors caused by inaccuracies in the stored energy-rate data and errors in the estimates of wind and temperature profiles.

The controls are throttle, nozzle, pitch, and roll angles. Flaps are not used as perturbation controls because of their relatively low rate limit and an operational constraint that flap motion be monotonic during an approach. The flap command is simply the reference value at each ground track position limited to the placard value at the current airspeed.

Lateral perturbation control is essentially uncoupled from the longitudinal mode and is accomplished through a roll-angle command to the roll-command autopilot. This command is of the form

$$\phi_c = \phi_r + k_{\phi y}\Delta y + k_{\phi \dot{y}}\Delta \dot{y}$$

where ϕ_r is the reference roll angle, and Δy and $\Delta \dot{y}$ are the crosstrack error and error rate, respectively. The two gains were chosen to provide a well-damped response and control activity compatible with the noise characteristics of the navigation system.

Longitudinal perturbation control for correcting airspeed and altitude errors is difficult because the reference controls generated by the energy-rate schedule of Fig. 1 often lie on a constraint boundary and therefore cannot be perturbed freely in both directions. The two controls that are often constraint limited during a fuel-conservative approach are throttle, π, and nozzle angle, ν. Some insight into this problem can be obtained using data from the energy-rate schedules. Figure 6 shows the energy-rate envelope from Fig. 1 with the minimum reference nozzle and minimum reference throttle constraint boundaries. These boundaries divide the envelope into four regions:
I, where ν cannot be reduced; II, where neither π nor ν can be reduced; III, where π cannot be reduced; and IV, where π and ν are free to move in either direction. The combinations of controls available for increasing and decreasing $\dot{E}_n$ in each region are indicated in the figure. Note that in region I nozzle could be used as an additional control variable for decreasing energy rate. However, this variable is not used because throttle and pitch provide adequate control of flight-path errors in this region. In region IV the minimum reference throttle is above idle and is determined by the maneuver margin constraint. At each airspeed in this region the negative throttle perturbation that can be added to the reference throttle to yield the commanded throttle is limited to -2% for safety reasons. Positive and negative throttle perturbations are further limited so that the commanded throttle, π_c, falls in the engine operating range, $84\% \leq \pi \leq 96\%$.

The perturbation equations and the perturbation control law can be written in state vector notation as

$$\frac{dx}{dt} = Fx + Gu \qquad (14)$$

$$u = Kx \qquad (15)$$

where

$$x = (\Delta V, \Delta\gamma, \Delta h, \int \Delta V dt, \int \Delta h dt)^T$$

$$u = (\Delta\pi, \Delta\theta, \Delta\nu)^T$$

The delta quantities are the perturbations from reference values, i.e., $\Delta V = V_a - V_{ar}$, etc., where V_a is the aircraft and V_{ar} the reference true airspeed, respectively. The commanded controls are the sum of reference and perturbation controls.

$$u_c = (\pi_r + \Delta\pi, \theta_r + \Delta\theta, \nu_r + \Delta\nu) \qquad (16)$$

For a powered-lift STOL aircraft such as the one used for these flight tests, the values of F and G are strongly dependent on airspeed and energy rate and are thus time-varying along a trajectory. Quadratic Optimal Synthesis[5] would therefore yield time-varying gain matrices that are also functions of the reference trajectory. But it is neither practical nor necessary to implement a complex, reference-trajectory-dependent gain matrix in order to achieve adequate control system performance in this case.

The design procedure employed here began by first computing optimum gain matrices at various operating points in the control region diagram (Fig. 1) using fixed values of F and G. The analysis of these gain matrices showed the strongest dependence on airspeed, reference nozzle angle, and reference flaps. Sensitivity of the closed-loop eigenvalues to changes in several of the gains was low, allowing those to be set to zero or held constant throughout the operating region. It was possible to fit the variable gains with relatively simple functions of reference airspeed, nozzle angle, and flap angle. This method resulted in the following gain matrix:

$$K = \begin{bmatrix} \frac{-40}{V_{ar}} & \frac{-40}{V_{ar}} & \frac{-8}{V_{ar}} & \frac{-4\cos\phi_r}{V_{ar}} & \frac{-0.6}{V_{ar}} \\ 0 & -0.4 & \frac{-14}{V_{ar}} & 0 & \frac{-0.2}{V_{ar}} \\ 3 & 2 & 0.6 & 0.3 & 0.05\max\left\{0, \frac{\delta_f - 45°}{20}\right\} \end{bmatrix} \qquad (17)$$

where V_{ar} is in units of ft/sec. Extensive computer calculations have verified that the closed-loop eigenvalues of this system have damping factors of 0.707 or greater and real parts less than -0.05/sec at all operating points. These characteristics provide adequate tracking performance. When operating in region I of Fig. 6 the last row of K is set to zero since nozzle angle is not used for control. In regions II and III throttle perturbations are limited to positive values, while in region II nozzle perturbations are limited to positive values. In region IV each control moves freely, but negative throttle perturbations are limited to -2% RPM, as previously explained. Control limiting can reduce the effectiveness of integral feedback of speed and altitude. Some design considerations for these integral feedback loops are given in Ref. 9.

The throttle and nozzle angle perturbations generated by the control law will generally be of opposite sign, because the elements of the first row of K all have opposite sign of the third row elements. Thus, even in region II, where throttle and nozzle perturbations are each limited to move only in the positive direction; they are not generally limited simultaneously. This implies that two controls, either throttle and pitch or nozzle and pitch, are free to move. Transient response studies using a nonlinear simulation of the aircraft and guidance system have shown that the control power is adequate to provide rapid and well-damped airspeed and altitude error responses in region II. Example transient responses from this simulation are discussed in the last section.

Structure and Operation of the Flight System

The integration of the functional units of the system is shown in Fig. 7. Computations begin in the fast time trajectory synthesis module. If a trajectory is successfully synthesized, it is stored at command points, as previously explained, and the synthesized horizontal trajectory is displayed to the pilot on an electronic Horizontal Map Display (HMD). This display operates in conjunction with the navigation system to give a map-like view of the terminal area (see Ref. 2 for details on this device). If the track switch is engaged, real-time profile generation and closed-loop tracking of the synthesized trajectory begins. The four control variables generated by the perturbation feedback law drive the roll and pitch autopilots and the throttle and vectoring nozzle servos.

Figure 8 gives an example of trajectories displayed on the HMD. The solidly drawn track is a fixed and prestored reference trajectory on which waypoint numbers are indicated. The pilot selects the waypoint on the fixed reference trajectory he wishes to capture by keyboard entry (waypoint 2 in this case). The track drawn with broken lines from P_1 to 2 indicates to the pilot that a valid capture trajectory to that waypoint has been computed. If the synthesis had not been successful, the synthesis routine would have been reentered, as shown in Fig. 7, with updated aircraft states as the new initial conditions.

To account for the distance the aircraft will travel while the trajectory is being synthesized and to give the pilot time to push the track switch, the capture trajectory is actually computed from P_2 rather than from the aircraft position at P_1 (see Fig. 8). The short, straight segment between P_1 and P_2 is referred to as a lead distance and it is drawn along the aircraft velocity vector at the start of synthesis. This technique minimizes initial condition errors at the beginning of the automatic-tracking mode.

After the reference trajectory has been stored and valid navigation data from TACAN† or MODILS‡ are received the track switch (see Fig. 7) is armed, ready for the pilot to engage. If the pilot does not engage the track switch before the aircraft reaches P_2, P_2 is moved to its new position, and a new capture trajectory is displayed if one were successfully computed. When the pilot engages the track switch as at P_1 in Fig. 8, the capture path on the display is drawn with a solid line indicating to the pilot that closed-loop guidance to the synthesized trajectory has begun.

While the capture-trajectory algorithm synthesizes successful trajectories for a wide range of initial conditions, there are conditions where it will fail to do so. For example, if P_1 is very close to the capture waypoint, then the algorithm can fail because there is insufficient distance along the computed minimum distance path to complete the required change in the speed and/or altitude. In that case, the reason for the failure to synthesize is displayed as a short message on the HMD. The pilot can correct the failure to capture condition by flying the aircraft away from the capture waypoint or by selecting a more distant capture waypoint.

The fixed reference trajectory, though not always usable as explained in the introduction, prescribes a nominal approach route and is determined by air-traffic control and terminal-area constraints. The precise airspeed and altitude profiles along this fixed reference usually are not rigidly specified. Often the airspeeds and altitudes are specified only at waypoints. In that case the speed and altitude profiles between adjacent waypoints are synthesized in fast time using the same algorithm as for the capture trajectory. The synthesis is done in backward time starting at the last waypoint and ending at the capture waypoint. The altitude and speed at waypoint N-1 determine the final condition and the altitude and speed at waypoint N determine the initial condition for the synthesis. Thus, every available degree of freedom is exploited to optimize the total trajectory.

Simulation and Flight Test Results

The performance of the guidance system was evaluated in simulation and flight tests. The piloted simulator was the primary tool for determining the performance limits of the system since it allowed the measurement of performance for known disturbance inputs. In flight, it is difficult to measure or control disturbances and isolate their effect on performance. Flight tests were used to verify the simulator model and to obtain pilot comments on the operational acceptability of the system.

Figure 9(a) gives simulator time histories of selected states and controls for a combined capture and fixed approach trajectory, from 3000 ft altitude, 140 KEAS, and 40,000 ft to touchdown. The

---

†TACtical Air Navigation System provides azimuth and range relative to station location.

‡MODular Instrument Landing System is an interim microwave landing system with a azimuth scan of ±20°, an elevation scan of 16°, and a precision distance measuring system with a range of 10 n. mi.

initial position and heading were chosen to yield a more or less straight-in horizontal capture path along the extended centerline of the runway. Waypoint 2 of the fixed-reference path shown in Fig. 8 was selected as the capture waypoint. The capture trajectory consists of a constant speed, level flight segment to point A where a -7.5° descent begins. Deceleration at 0.05 g starts at point B while the aircraft is in descent. The deceleration is initiated by starting the deployment of flaps (not shown in the figure). End of capture and the start of the final-approach trajectory is at point C, which corresponds to waypoint 2 in Fig. 8, where the aircraft has decelerated to the landing speed of 72 KEAS and is tracking a -7.5° glide slope. Point C is 700 ft above the runway and about 5400 ft from touchdown. Automatic tracking is terminated at point D (Waypoint 1 in Fig. 8), 300 ft above the runway and 2280 ft from the nominal touchdown point. The capture trajectory was synthesized using a minimum flight-path angle of -7.5° and a maximum deceleration of 0.05 g. The parameters σ and ε were set to 0.9 and 1.0, respectively. The choice of $\varepsilon = 1$ gives the priority to deceleration during the combined deceleration and descent segments. This combination of limits and parameter values resulted in a reduction in flight-path angle from -7.5° to -6.9° for a 10 sec period just prior to point C. Both the synthesis algorithm and the aircraft simulator assumed zero wind speed, a standard temperature profile, and an aircraft weight of 48,000 lb. Navigation errors were set to zero. The tracking performance of the perturbation-control law under these nominal conditions serves as a standard against which the performance under off-nominal and flight-test conditions can be evaluated.

The step throttle reduction to 84% RPM and the pitch-down command (not shown in Fig. 9a) lead the computed descent point at point A by about 6 sec to compensate for throttle- and pitch-angle dynamics. This prevents overshoots in tracking the reference altitude at the point of descent. The small altitude transient at this point is damped in about 5 sec. Speed and altitude errors during the deceleration and descent segment between points B and C never exceed 4 knots and 20 ft, respectively. These errors converge to zero between points C and D. Though of no practical significance, the residual errors during deceleration are caused by inaccuracies in the reference throttle, nozzle, and pitch commands computed from the energy rate performance tables during fast time synthesis. The response of the perturbation control law to these modeling inaccuracies is seen as the difference between the superimposed traces of commanded and reference nozzle and throttle angles in Fig. 9a. These differences are small even while reference nozzle and throttle angles are increasing rapidly toward the end of the decleration segment. The validity of the energy-rate-performance model as an accurate predictor of aircraft performance during these quasi-dynamic maneuvers is thus verified.

Figure 9b shows the control system response to a 10-knot headwind pulse of about 70-sec duration using the same reference trajectory as in Fig. 9a. The initial speed error resulting from this pulse is rapidly damped by using the nozzle as control. Then, integral speed and altitude feedback develops throttle-, nozzle-, and pitch-perturbation biases in about 20 sec to correct the reference controls for the change in aerodynamic flight-path angle caused by the change in the mean wind. In effect, the integral feedback serves as an estimator of the mean wind. When the headwind pulse is removed just after point C, the effect is equivalent to a tailwind pulse and results in another transient. Note that the introduction of the headwind pulse has increased the time between points B and C because the ground speed is reduced. Crosstrack position errors, though not shown, remain negligibly small during the approach.

Other simulation results have shown that the control law can compensate for unmodeled tailwinds and headwinds of 15 and 25 knots, respectively, without excessive control saturation. Also, errors of 10% in aircraft weight and +20° C and -10° C unmodeled temperature deviations from that assumed are compensated by the control law.

Figure 10 shows various time histories for a straight-in flight-test approach under conditions similar to those in the simulations. One significant difference was the use of .03 g maximum deceleration in the flight test. This caused the deceleration to begin at point A before the point of descent at B. The entire approach trajectory was flown using TACAN for navigation. The location of the TACAN station relative to the runway is shown in Fig. 8. Because of its favorable location, the TACAN station provided sufficient navigation accuracy for flying the approach without switching to the higher precision MODILS as would normally be required. There was light to moderate turbulence and an average headwind of about 15 knots below 4000 ft as measured by a radar-tracked weather balloon just prior to takeoff. However, the wind profile was not entered into the synthesis logic and thus constituted an unmodeled wind. Altitude errors, except near the pitch-down point, did not exceed 35 ft and decreased to about 15 ft near the end. Speed errors during deceleration were less than 10 ft/sec, and decreased to about 1 ft/sec at the end. If allowance is made for the presence of turbulence, winds, and navigation-system noise during the flight, these errors agree reasonably well with the simulation results and are acceptably low. The control perturbation biases, evidently caused by modeling errors and the unmodeled wind, are larger than those seen in the simulation run of Fig. 9a, though they are not excessive. Nozzle bias during the middle of the deceleration averages about 25°. While this seems large it should be noted that during this interval the throttle is at flight idle, where the effect of nozzle on energy rate is a minimum. On the whole, the control biases represent fairly small errors in the energy rate model. The flight-test results can, of course, be used to improve the accuracy of the energy-rate model of the aircraft.

The crosstrack error at point D measured by precision radar was 80 ft or less than half the width of the runway. This error, which the pilot can null during manual flight from point D (waypoint 1) to touchdown, approaches the accuracy limits of TACAN. At the same time it sets a lower limit on the distance between point D and touchdown when using TACAN. Pilots judged the action of the control law as smooth and the capture trajectory as a convenient and effective tool for optimizing approach trajectories.

The fuel consumption of this automatically flown trajectory was compared with that of a trajectory flown by a test pilot under simulated instrument-flight-rule conditions. In order to provide a basis for comparison the manually flown trajectory began from the same initial distance-to-touchdown, airspeed and altitude as the automatically flown trajectory. The approach was made with the aid of a flight-director system which displayed to the pilot lateral and longitudinal deviations from a straight-in, 7.5° approach path. The fuel used for the automatic approach was 381 lb, while that for the manually flown one was 500 lb. Further simulations and flight tests should be conducted to compare the fuel consumption for various approach trajectories, flight-director designs, and wind conditions before the fuel conservation potential of this guidance system can be considered established.

Concluding Remarks

The automatic guidance system described in this paper achieves the dual goal of fully automatic flight and near-optimal fuel conservation through the technique of fast-time onboard trajectory synthesis. This technique overcomes the performance limitations inherent in a stored, precalculated trajectory by adapting the trajectory to the unique conditions encountered in each landing approach. The ability to adapt is crucial in the terminal area since the initial conditions for starting the approach and the wind and temperature profiles are not predictable with sufficient accuracy prior to takeoff. The technique for synthesizing the trajectories allows the pilot to choose various deceleration/descent profiles. All profiles have the common characteristic of delaying the start of the descent and deceleration points as much as possible. A preliminary flight evaluation indicates that an automatically flown, optimum approach can produce significant fuel savings relative to an approach flown manually with only conventional flight-director guidance. The design procedure described herein for a STOL aircraft is applicable with lesser control complexity to guidance system design for CTOL aircraft.

References

[1]Neuman, Frank, Watson, Delamar M., and Bradbury, Peter, "Operational Description of an Experimental Digital Avionics System for STOL Airplanes, NASA TM X-62,448, Dec. 1975.

[2]Lee, Homer Q., Neuman, Frank, and Hardy, Gordon G., "4D Area Navigation System Description and Flight Tests," NASA TN D-7874, Aug. 1975.

[3]Bryson, A. E., Jr., Desai, M. N., and Hoffman, W. C., "Energy State Approximation in Performance Optimization of Supersonic Aircraft," Journal of Aircraft, Vol. 6, Nov.-Dec. 1969.

[4]Erzberger, Heinz, and Lee, Homer Q., "Terminal-Area Guidance Algorithms for Automated Air Traffic Control," NASA TN D-6773, April 1972.

[5]Pecsvaradi, Thomas, "Four-Dimensional Guidance Algorithms for Aircraft in an Air Traffic Control Environment," NASA TN D-7829, March 1975.

[6]Erzberger, Heinz, McLean, John D., and Barman, John F., "Fixed-Range Optimum Trajectories for Short-Haul Aircraft," NASA TN D-8115, Dec. 1975.

[7]Jakob, Heinrich, "An Engineering Optimization Method with Application to STOL Aircraft Approach and Landing Trajectories," NASA TN D-6978, Sept. 1972.

[8]Bryson, A. E., Jr. and Ho, Y. C., "Applied Optimal Control", Blaisdell Publishing Co., 1969.

[9]Slater, Gary, "Analysis of Integral Controls in Linear Quadratic Regulator Design." AIAA Guidance and Control Conference, Aug. 6-8, 1979, Boulder, Colorado, pp. 79-1743.

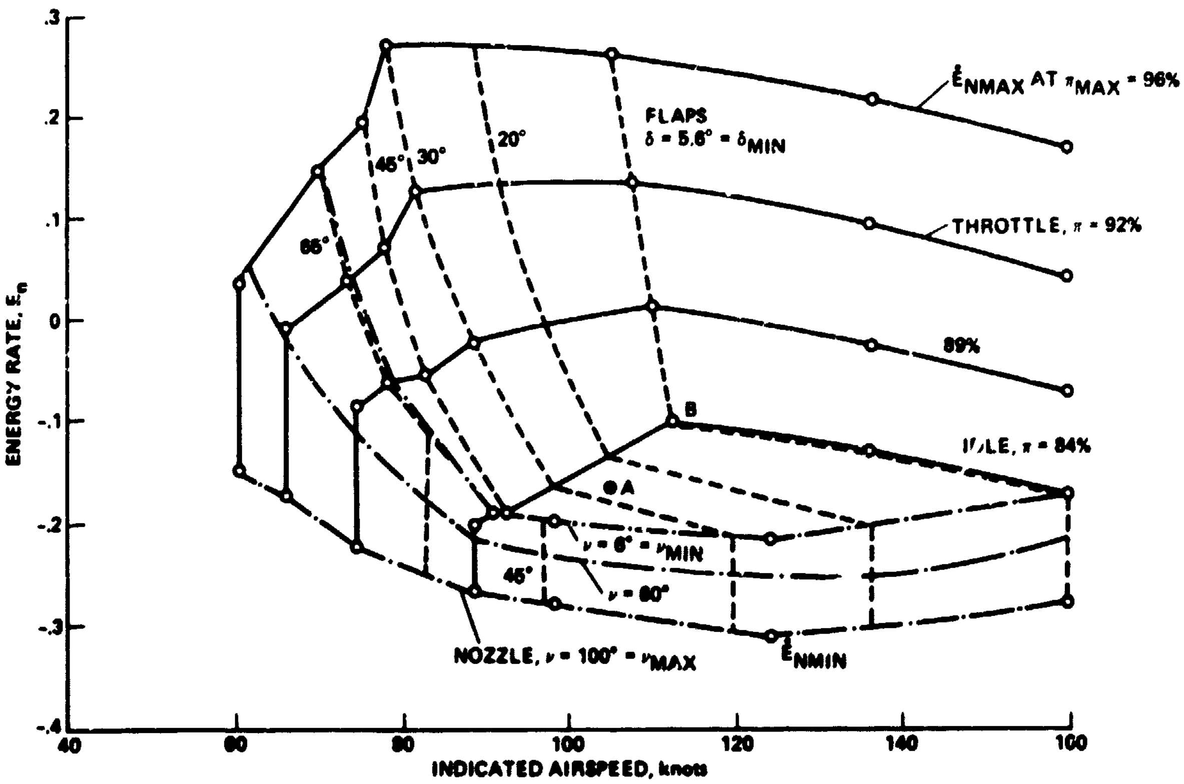

Fig. 1 Energy rate diagram for STOL aircraft; W = 38,000 lb, sea level 59° F.

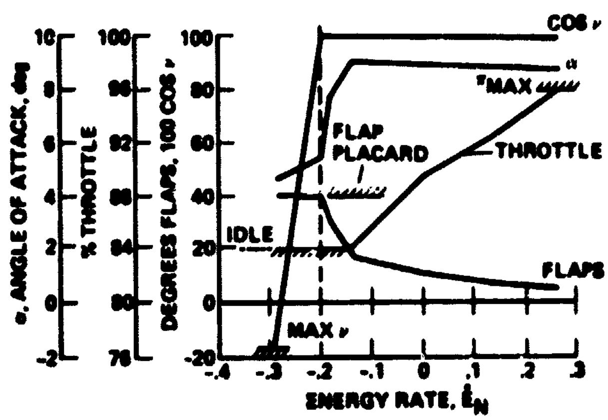

Fig. 2 Optimum controls as function of energy rate at 105 knots; W = 38,000 lb, sea level, 59° F.

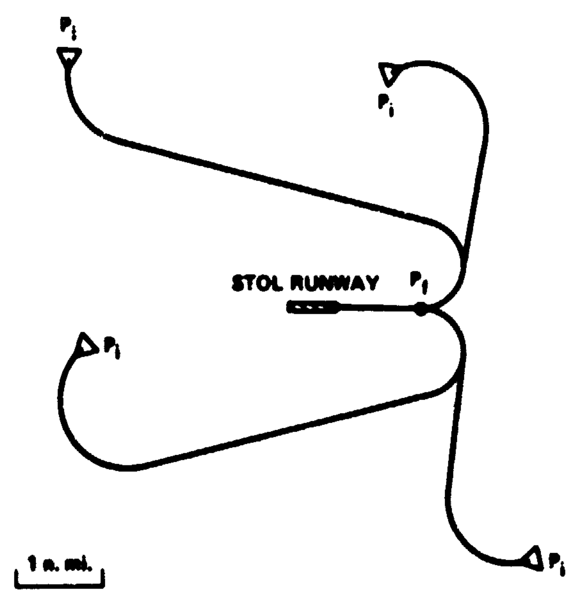

Fig. 3 Examples of minimum distance, constant turn radius, horizontal capture trajectories to a capture point P_f on final approach.

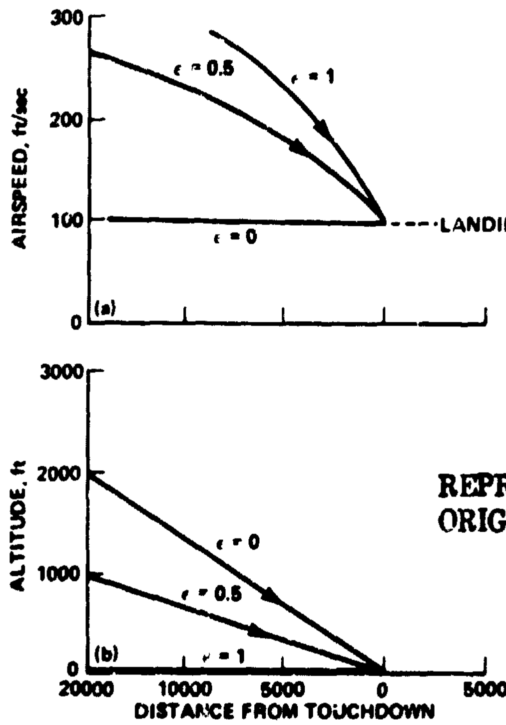

Fig. 4 Effect of ε on speed and altitude profiles, with $\dot{E}_n$ ..13.

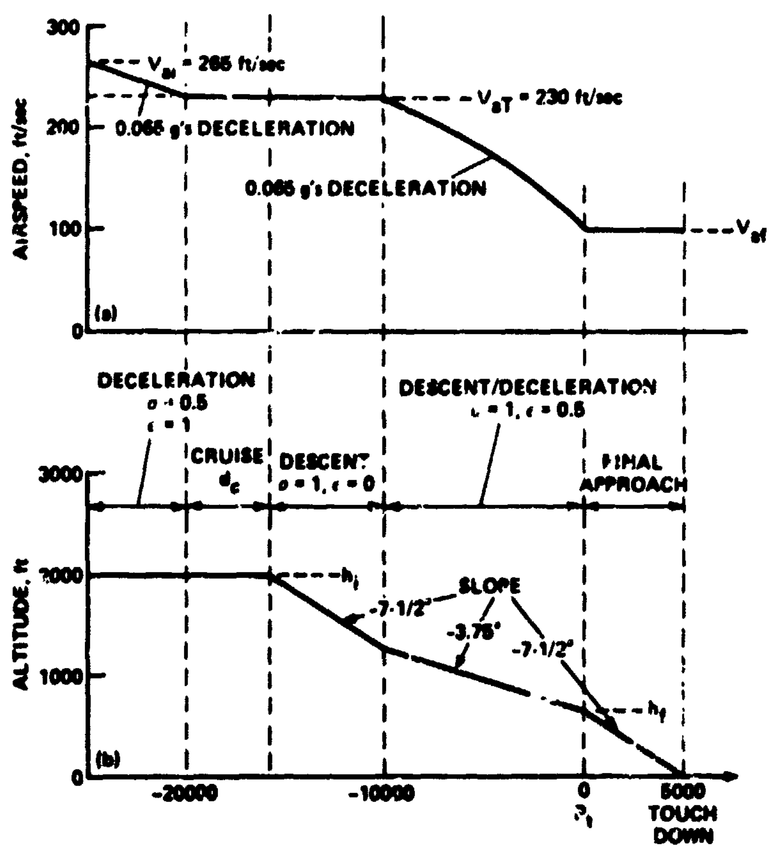

Fig. 5 Example of synthesized STOL approach trajectory.

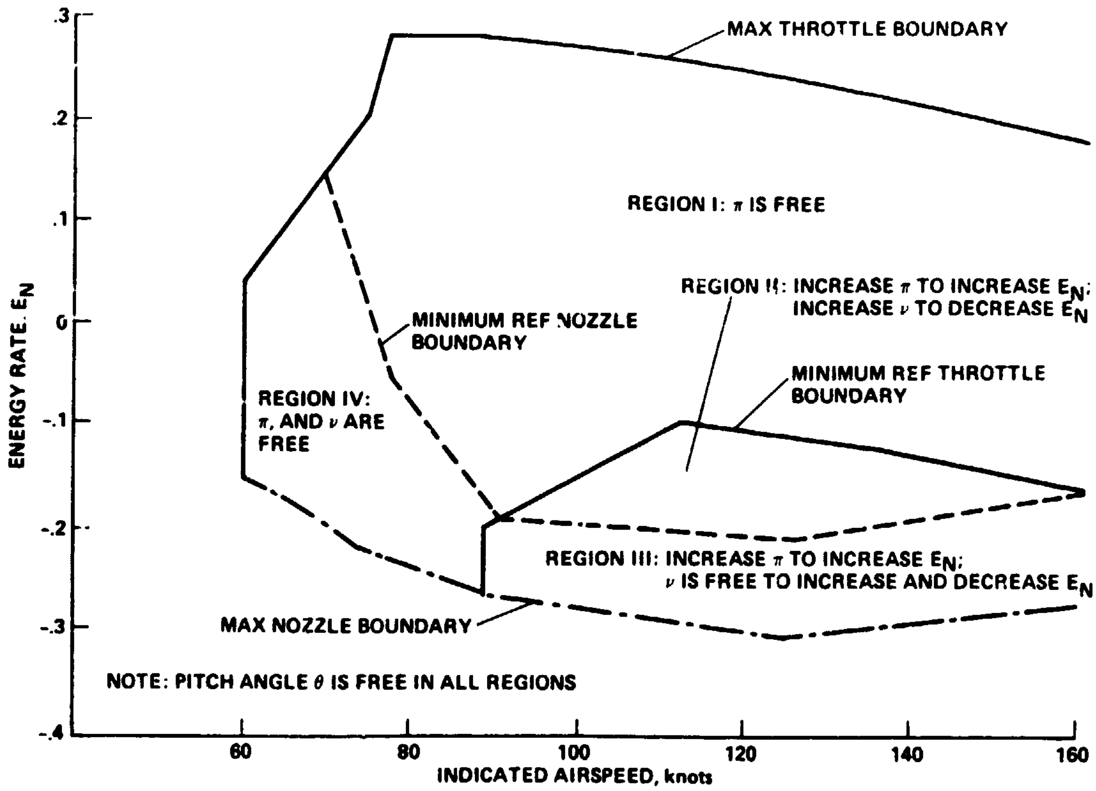

Fig. 6 Constraint boundaries for perturbation controls.

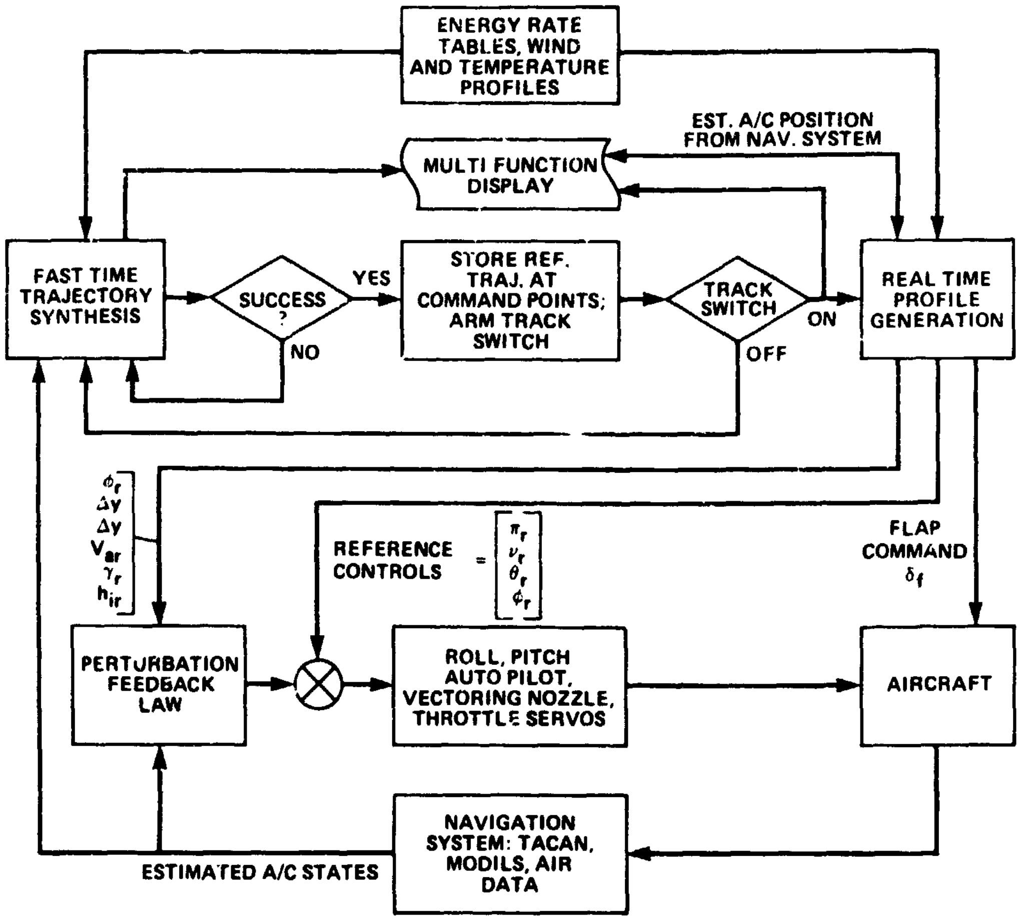

Fig. 7 Block diagram of guidance system.

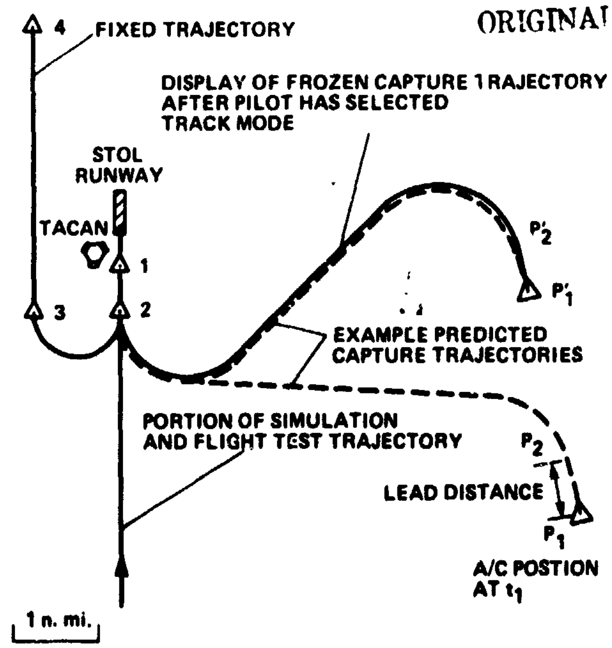

Fig. 8 Horizontal flight paths displayed on cockpit Horizontal Map Display (HMD).

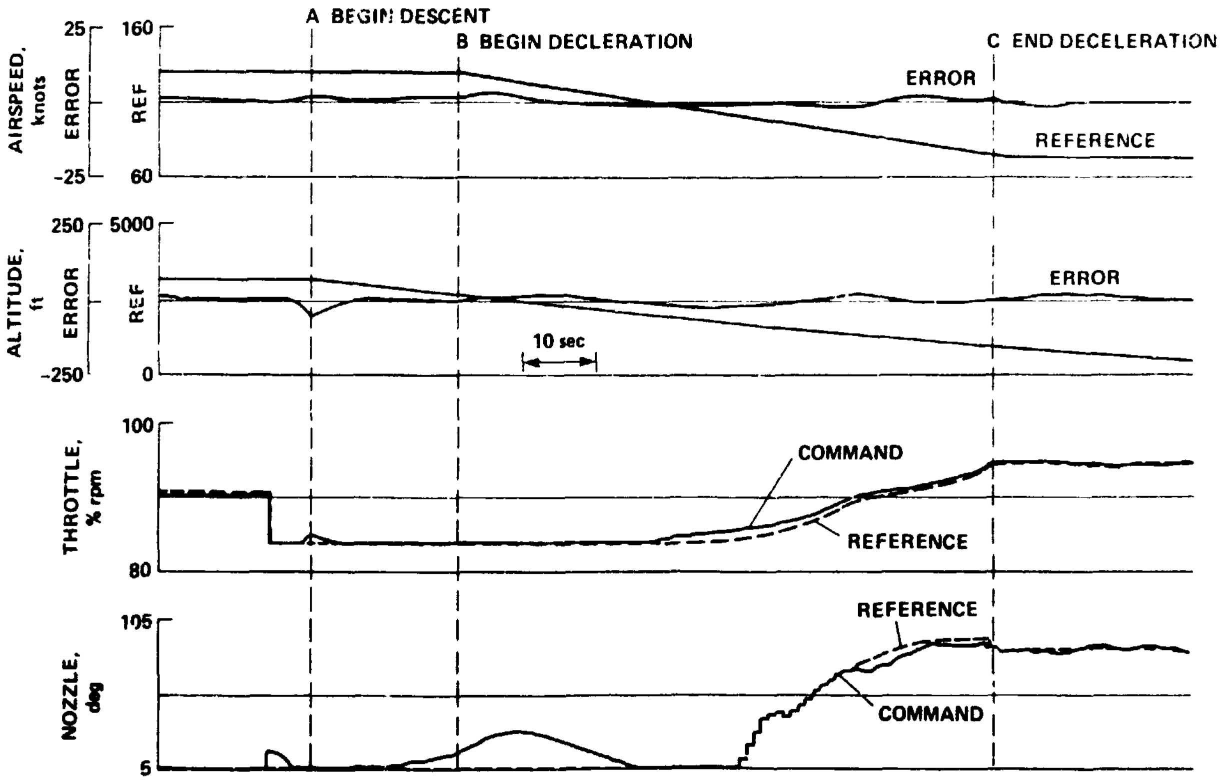

(a) Nominal conditions.

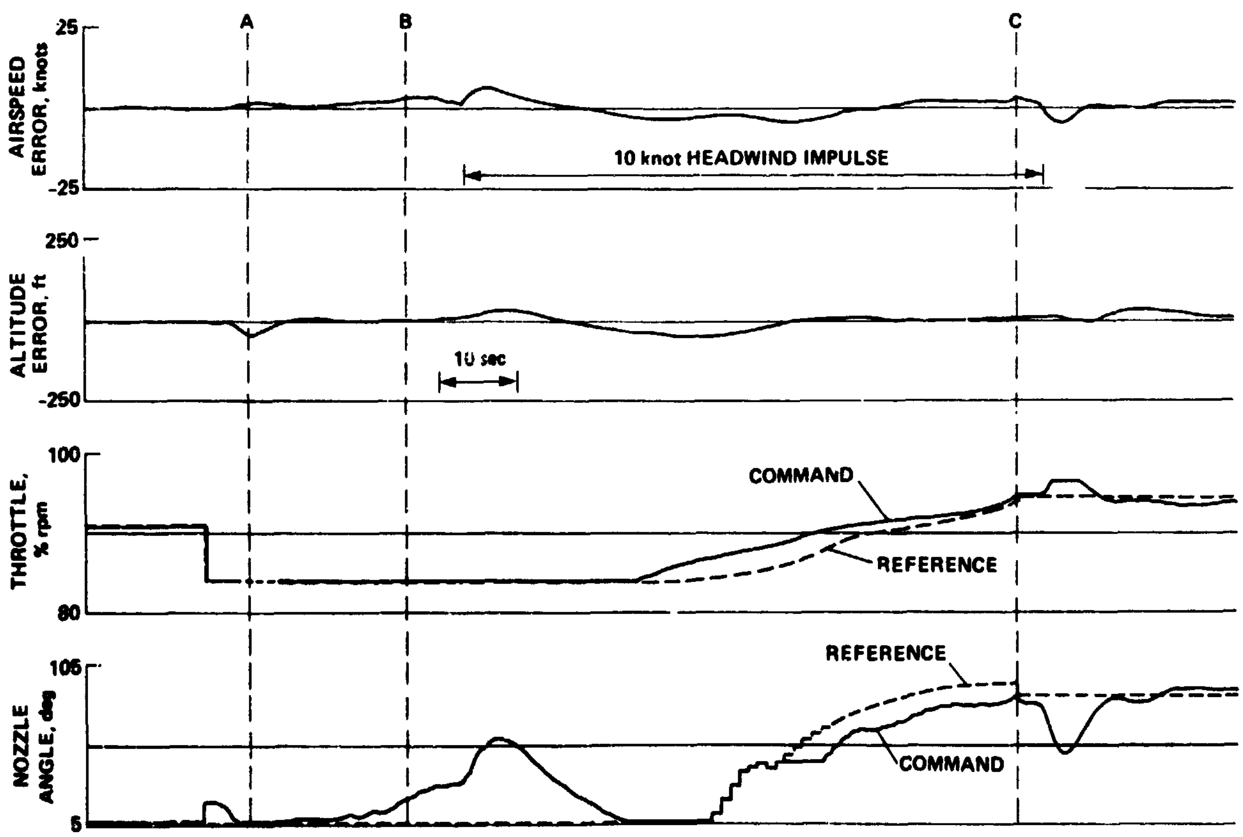

(b) Effect of 10-knot headwind impulse.

Fig. 9 Simulation of typical approach trajectory; runway at 140-ft A.S.L.

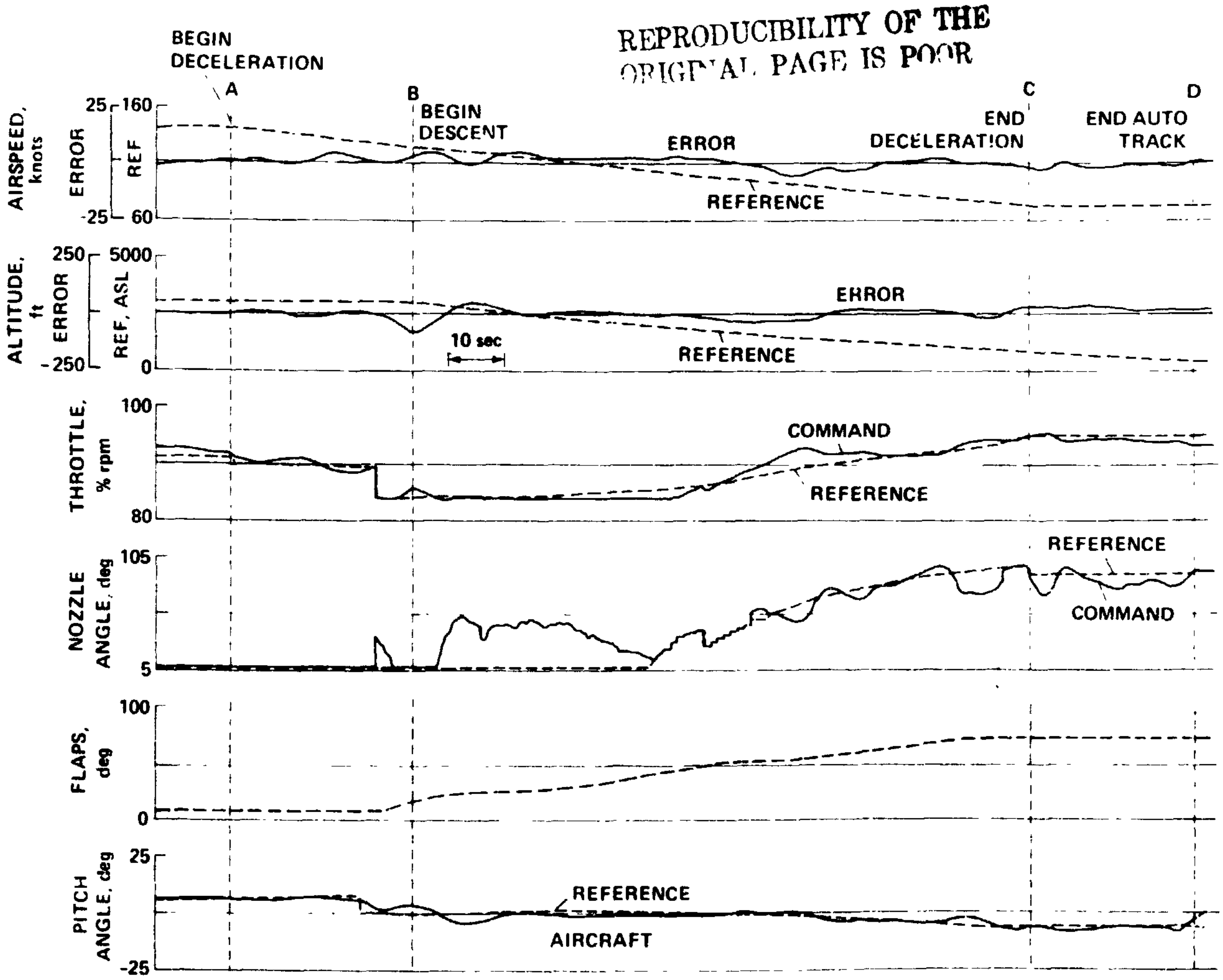

Fig. 10 Flight-test results, runway at 140-ft A.S.L.

1. Report No.	2. Government Accession No.	3. Recipient's Catalog No.
NASA TM-78595		

4. Title and Subtitle	5. Report Date
FUEL-CONSERVATIVE GUIDANCE SYSTEM FOR POWERED-LIFT AIRCRAFT	
	6. Performing Organization Code
7. Author(s)	8. Performing Organization Report No.
Heinz Erzberger and John D. McLean	A-7860
9. Performing Organization Name and Address	10. Work Unit No.
Ames Research Center, NASA Moffett Field, Calif. 94035	505-07-11
	11. Contract or Grant No.
12. Sponsoring Agency Name and Address	13. Type of Report and Period Covered
National Aeronautics and Space Administration Washington, D.C. 20546	Technical Memorandum
	14. Sponsoring Agency Code

15. Supplementary Notes

Paper for AIAA Guidance and Control Conference, Aug. 6-7, 1979, Boulder, CO.

16. Abstract

A concept for automatic terminal-area guidance, comprising two modes of operation, has been developed and evaluated in flight tests. In the first or predictive mode, fuel efficient approach trajectories are synthesized in fast time. In the second or tracking mode, the synthesized trajectories are reconstructed and tracked automatically. An energy rate performance model derived from the lift, drag, and propulsion system characteristics of the aircraft is used in the synthesis algorithm. The method optimizes the trajectory for the initial aircraft position and wind and temperature profiles encountered during each landing approach. The paper describes the design theory and discusses the results of simulations and flight tests using the Augmentor Wing Jet STOL Research Aircraft.

17. Key Words (Suggested by Author(s))	18. Distribution Statement
Aeronautics Navigation Guidance	Unlimited STAR Category - 01

19. Security Classif. (of this report)	20. Security Classif. (of this page)	21. No. of Pages	22. Price*
Unclassified	Unclassified	17	$3.50

*For sale by the National Technical Information Service, Springfield, Virginia 22161